

Significance of nuclear quantum effects in hydrogen bonded molecular chains

Aleš Cahlík^{1,2,3†}, Jack Hellerstedt^{1,†}, Jesús I. Mendieta-Moreno^{1†}, Martin Švec^{1,3}, Vijai M. Santhini¹, Simon Pascal⁴, Diego Soler-Polo⁵, Sigurdur I. Erlingsson⁶, Karel Výborný¹, Pingo Mutombo^{1,8}, Ondrej Marsalek⁷, Olivier Siri^{4*}, Pavel Jelínek^{1,3*}

¹Institute of Physics of the Czech Academy of Sciences, v.v.i., Cukrovarnicka 10, CZ-16200 Prague 6, Czech Republic

²Faculty of Nuclear Sciences and Physical Engineering, Czech Technical University in Prague, Břehová 78/7, CZ-11519 Prague 1, Czech Republic

³Regional Centre of Advanced Technologies and Materials, Palacký University, Šlechtitelů 27, CZ-78371 Olomouc, Czech Republic

⁴Aix Marseille Univ, CNRS, CINaM, UMR 7325, Campus de Luminy, F-13288 Marseille Cedex 09, France

⁵Universidad Autónoma de Madrid, Campus Cantoblanco, Madrid, Spain

⁶School of Science and Engineering, Reykjavik University, Menntavegi 1, IS-101 Reykjavik, Iceland

⁷Charles University, Faculty of Mathematics and Physics, Ke Karlovu 3, CZ-12116 Prague 2, Czech Republic

⁸Department of Petrochemistry and Refining, University of Kinshasa, Kinshasa, Democratic Republic of Congo

*Correspondence to: olivier.siri@univ-amu.fr, jelinekp@fzu.cz

†These authors contributed equally to this work.

Abstract:

In hydrogen bonded systems, nuclear quantum effects such as zero-point motion and tunneling can significantly affect their material properties through underlying physical and chemical processes. Presently, direct observation of the influence of nuclear quantum effects on the strength of hydrogen bonds with resulting structural and electronic implications remains elusive, leaving opportunities for deeper understanding to harness their fascinating properties.

We studied hydrogen-bonded one-dimensional quinonediimine molecular networks which may adopt two isomeric electronic configurations via proton transfer. Herein, we demonstrate that concerted proton transfer promotes a delocalization of π -electrons along the molecular chain, which enhances the cohesive energy between molecular units, increasing the mechanical stability of the chain and giving rise to new electronic in-gap states localized at the ends.

These findings demonstrate the identification of a new class of isomeric hydrogen bonded molecular systems where nuclear quantum effects play a dominant role in establishing their chemical and physical properties. We anticipate that this work will open new research directions towards the control of mechanical and electronic properties of low-dimensional molecular materials via concerted proton tunneling.

TEXT:

Nuclear quantum effects (NQEs), such as proton tunneling and zero-point motion can play an important role in understanding structural¹ and material properties²⁻⁴ of hydrogen-bonded systems at low temperatures. It has been demonstrated both theoretically⁵ and experimentally⁶ that nuclear quantum effects may have a pronounced two-fold effect on the strength of hydrogen bonds, either further weakening of already weak hydrogen bonds or conversely, strengthening of the relatively strong ones. NQEs can induce strong proton delocalization with direct consequences on chemical activity of system.⁷ Complex, concerted many-body proton motion in ice has been described both experimentally⁸ and theoretically^{9,10}. In this context, recent progress in scanning probe microscopy providing unprecedented spatial resolution on single molecules via a proper tip functionalization^{11,12} has enabled the direct observation of concerted proton motion in water tetramers¹³.

Despite these advances, our present understanding of NQEs remains incomplete. In this work, we show that the concerted proton motion in a H-bonded 1D molecular system not only enhances its mechanical stability but directly modifies its electronic structure, forming new electronic in-gap states localized at the ends of the chain.

2,5-diamino-1,4-benzoquinonediimines (DABQDI, structure in Fig.1a inset) belong to a family of quinoid molecules with intriguing electronic properties¹⁴ stemming from a unique distribution of their π -electrons. DABQDI quinones contain 12 π -electrons which can be perceived as two independent π -subsystems containing 6 conjugated π -electrons (the nitrogen lone pair is conjugated with the two double bonds), chemically linked via two C-C σ -bonds, but electronically not conjugated^{15,16}. The molecular DABQDI building blocks exist in solution as two tautomers in equilibrium, whose mutual alternation can be realized via a fast intramolecular

double proton transfer that generates a structure of higher symmetry (i.e. an averaged form of the two tautomers) which directly alters the π -conjugation of the whole DABQDI molecule.¹⁷ Curiously, although unsubstituted DABQDI (N-H) was reported in the literature in 1887¹⁸, this molecule has since rarely been investigated, probably due to its very low solubility and poor stability (co-condensation, hydrolysis, and oxidation side reactions).¹⁹

Here we explore self-assembled molecular chains built from the precursor DABQDI on a metallic Au(111) surface at low temperatures (5 K) under ultra-high vacuum conditions. The presence of imine (as H-acceptor) and amine groups (as H-donor) enables, in principle, the formation of 1D intermolecular hydrogen-bonded assemblies. Such chains may adopt two isomeric π -conjugations resulting from the distinct alternation of double and single bonds according to the position of the amine group hydrogen atoms. In principle, the energy landscape of the system can be mimicked by a symmetric double-well potential, which has different ground states in either the classical or quantum picture. While in the classical picture the system is localized in one of the wells, the quantum ground state exists as a superposition of two states²⁰. As we will show later on, the quantum state strongly affects the electronic structure of the chain. In this one-dimensional configuration, the presence of concerted proton transfer not only induces resonant tunneling between the two degenerate π -conjugated electronic states of the chain, but it also mediates an effective coupling of the π -electron systems across the chain. This coupling of resonant electronic configurations leads to the emergence of new electronic states and reinforcement of the mechanical stability of the molecular chain.

Figure 1a shows a representative overview scanning tunneling microscopy (STM) image acquired at 5 K of linear self-assembled 1D molecular structures, which form upon deposition of DABQDI molecules on the Au(111) surface at room temperature. Typically, we observe chains with lengths ranging between 3 and 100 nm, oriented independently of the surface herringbone reconstruction. The hallmark of these molecular chains is the presence of characteristic bright spots in STM images located at the ends of the chains, as can be seen in Fig. 1b. In addition to the chains, distinct individual molecular species are present on the substrate, predominantly

situated on the herringbone elbows, which we identify as individual molecules containing an extra proton as will be discussed later.

We are readily able to contact and manipulate complete chains along the surface by approaching the tip to a chain end with a subsequent lateral tip movement. Figure 1c displays a series of STM images of the same chain acquired between consecutive manipulations (see also Supplementary Video 1). Chains always remained intact during manipulation, demonstrating a weak dispersive interaction between the molecular chains and the underlying metallic surface, and a relatively strong intermolecular binding. To our knowledge this is the first demonstration of supramolecular hydrogen-bonded systems being manipulated in a controlled way by a scanning probe without loss of structural integrity. This highlights the possible impact of proton tunneling on the strength of hydrogen bonding between the molecular units forming these chains. Indeed, the fact that NQEs may further enhance cohesion of relatively strong hydrogen bonds has been explored theoretically^{5,6}, but direct observations are lacking.

The picture is qualitatively different when the DABQDI molecules are sublimed at slightly elevated temperature and pressure (see Methods). The resulting molecular chains incorporate more defects, their growth is restricted by the herringbone reconstruction of the Au(111) surface and they lack bright end terminations, as can be seen in Extended Data Fig. 1a,b. Moreover, the mechanical stability is drastically reduced, making lateral manipulation impossible. Instead, mechanical interaction with the scanning probe easily splits the chains into segments, as shown in Extended Data Fig. 1d. For clarity, in the rest of the manuscript we will refer to the exemplary former species as symmetric chains while the latter will be referred to as canted chains.

To better understand the internal structure of the adsorbed chains and single molecular species, we acquired high-resolution atomic force microscopy (AFM) images with a CO-functionalized probe^{11,12}. This scanning probe technique has repeatedly demonstrated the unique capabilities of unambiguous discrimination of chemical structure,^{21,22} electrostatic potential mapping,²³ or identification of the spin state²⁴ of single molecules on surfaces.

The high-resolution AFM image of a single molecular species, not participating in the chain formation, shown in Fig. 2a, reveals a characteristic trapezoidal shape. Perfect agreement of the experimental AFM image with the simulation based on the chemical structure shown in Fig. 2b

can be achieved by including the presence of an extra hydrogen in the single molecule species (Fig. 2c, d). The detailed structure of the hydrogenated molecule as well as the origin of the extra hydrogen are discussed in the Supplementary Information. We presume this additional hydrogen impedes an efficient self-assembling process via hydrogen bonding with the remaining molecules (the H-acceptor capability is suppressed).

Figure 2e presents high resolution AFM images of the symmetric chain interior. By registering the molecular structure with the underlying Au(111) surface we determined the distance between two contiguous molecules to be 8.0 ± 0.1 Å. This excludes the possibility of covalent bonding, since the Density Functional Theory (DFT) calculated periodicity of a chain composed of covalently bonded molecules is significantly lower (5.7 Å, see Extended Data Fig. 2a). The absence of any repulsive signal in the AFM images between molecular units rules out the presence of a metal atom (such as gold, Extended Data Fig. 2b) and consequently a dative bonding motif in the chain. A classical total energy DFT calculation of a molecular DABQDI chain assembled by hydrogen bonds (Fig. 2k, l) provides relatively good agreement but with slightly larger distance between two adjacent molecules (8.12 Å), further disfavoring the dative hypothesis. However, molecules in such chains are canted with respect to the main chain axis in order to decrease the energy by aiming the hydrogens participating in the hydrogen bond toward their respective nitrogen atoms. This is in contrast with the experimentally observed symmetric chain structure where all the molecular units are symmetric around the main axis (see Fig. 2e). We resolved this inconsistency by using Path Integral Molecular Dynamics (PIMD) simulations (details later) which account for NQEs (corresponding atomic structure shown in Figure 2g). The calculated intermolecular distance using average atomic positions of PIMD calculations, 8.03 Å, fits very well to the experimental value (8.0 ± 0.1 Å). Moreover, the corresponding simulated AFM image (Fig. 2f) shows a highly symmetric arrangement caused by slight rearrangement of the atomic positions of hydrogens and nitrogens driven by the proton tunneling, which agrees very well with the experimental evidence.

On the other hand, the high-resolution AFM images acquired on canted chains (see Fig. 2i) match the AFM simulation (Fig. 2j) of the canted structure predicted by the total energy DFT simulations (Fig. 2k). This indicates that in the canted chains the molecular units are frozen in

one of the two possible configurations, while the symmetric chains are a superposition of the two degenerate electronic states that is driven by proton tunneling between adjacent nitrogen atoms. One possible way to confirm the relevance of the proton tunneling would be to carry out the same experiment with molecules synthesized using six deuterium atoms. Unfortunately, deuterated DABQDI molecules are chemically unstable, rendering such an experiment unfeasible.

To overcome this experimental limitation, we have performed PIMD simulations in order to elucidate the importance of NQEs and their impact on the structural properties of the molecular chains. We analyzed the results obtained from QM/MM (Quantum Mechanics/Molecular Mechanics) simulations²⁵ at different temperatures in which the quinone molecules were included in the QM region and the metallic surface is in the classical region. Figure 3a displays: 1) a free energy profile using our QM/MM (DFT) method treating all the nuclei as classical particles, and 2) quantum (PIMD) simulations of the concerted proton transfer between amine and imine groups within the chain at 20 K and 10 K, showing significant differences with respect to the classical free-energy profile at 10 K. The height of the quantum free-energy profile at 20 K decreases by approximately half with respect to the classical barrier and it is further lowered at 10 K. Moreover, the shape of the barrier also changes significantly, showing double well character with a concave dip in the central part of the barrier at 10 K, see Fig. 3a. This demonstrates that the NQEs cause strong proton delocalization across the tunneling barrier, revealing the presence of deep proton tunneling, as shown in Fig. 3b.

According to the quantum simulations, the intermolecular distance between two nitrogen atoms (3.03 Å) decreases with respect to the classical case (3.12 Å), facilitating the proton transfer. Moreover, NQEs not only change the spatial redistribution of hydrogens but also the adjacent nitrogen atoms, creating the symmetric atomic arrangement as shown on Fig. 3c. This symmetric atomic arrangement not only explains the observed AFM contrast of the chains (see Fig. 2e), but also facilitates more direct interaction between proton and nitrogen atoms, which alongside with the shortening of N-N bonds enhances the electrostatic interaction⁵. These effects may partially explain the experimentally observed mechanical stability of the symmetric chains.

To understand a detailed mechanism of the proton tunneling process, we analyzed the correlation between positions of individual protons during the tunneling transfer. Figure 3e shows the spatial distribution of δ -reaction coordinates of two selected hydrogen bonds against the average δ -coordinate of all the hydrogen bonds in the chain (for the definition of δ -reaction coordinates see Fig. 3d). The δ -coordinate distribution plots show two well-localized peaks, which correspond to the two isomeric π -conjugations. The particular diagonal position of the distribution peaks reveals the concerted motion of all the protons during the tunneling process. This concerted motion can be rationalized as a preservation of the appropriate π -conjugation of the systems, which would be violated by an asynchronous proton transfer that would consequently increase the total energy of the system. In contrast, pure proton transfer would again violate the π -conjugation, i.e. alternation of single and double bonds. Thus, proton transfer has to be accompanied by electronic rearrangement, and we can interpret the process as proton-coupled electron transfer²⁶ introducing a strong coupling between the electronic and vibrational proton degrees of freedom.

From this perspective, the ground state of the chain should be viewed as linear combination of two isomeric π -conjugations, which may effectively lead to the delocalization of π electrons over the chain. We note that the symmetric chains are characterized by the presence of bright spots at their ends, visible in STM imaging (Fig. 1b). To understand the origin of the bright spots, we performed point scanning tunneling spectroscopy (STS; see Methods) combined with high-resolution AFM imaging. This allows us to unambiguously correlate the chemical and electronic structure of the chain ends. Similar to the chain interior, the AFM image (Fig. 4b) shows a highly symmetric contrast supporting the presence of proton tunneling between two terminal nitrogen atoms. Figure 4d shows 1D STS spectroscopies taken along the central symmetry axis of the chain end (red dashed line, Fig. 4c), revealing the presence of an in-gap state tightly localized around the terminating molecule unit. The end-state is centered at 50 meV above the Fermi level. For the sake of clarity, selected spectra from spatial coordinates indicated in Fig. 4b are shown in Fig. 4a. This state only appears on the symmetric chain termination, remaining completely absent in the case of canted chains (see Extended Data Fig. 1 a, b). Thus, we attribute the appearance of the end-states (ESs) in the symmetric chains to the concerted proton tunneling motion, which allows the π -electron system to be effectively delocalized across the whole chain.

To understand the origin of the in-gap ESs, we analyzed the electronic structure of a tight-binding Hamiltonian mapping π -conjugated electrons of the chain (for detailed description see SI) as illustrated in Fig. 4e. First, we extracted tight-binding parameters representing π -electrons of an isolated molecule from our local basis DFT calculations²⁷ using the Löwdin transformation of p_z -orbitals only (the electronic spectrum of single molecule is shown in Fig. 4f left). We also introduced an intermolecular hopping τ_{hbond} between molecular units to the Hamiltonian (Fig. 4e), which in the case of classical H-bonds is much smaller ($\tau_{hbond} < 0.1\text{eV}$) than the hopping corresponding to covalent double or single bonds. Consequently, the electronic structure of a chain consisting of only weakly electronically coupled molecular units remains very similar to the single molecule case with only a slight broadening of the molecular levels into bands (see Fig. 4f). On the other hand, the presence of concerted proton tunneling with its strong proton-coupled electron transfer, enhances the electronic coupling of the π -electrons in the system. To consider these effects we introduced an extra hopping τ_{edge} between two nitrogen atoms at the edges of the chain, shown on Fig. 4e. We have analysed the influence of the parameters τ_{hbond} and τ_{edge} on the electronic spectrum of this model Hamiltonian. For certain values of the hopping parameters τ_{hbond} and τ_{edge} corresponding to weak covalent bonds (slightly weaker than intramolecular covalent bonds formed by π -electrons of carbon and nitrogen atoms), we find in-gap states (the electronic spectra shown in Fig. 4f, in-gap states highlighted by colors) spatially localized at the edges of the chain (Fig. 4g) in a good agreement with the experimental evidence. In this way the experimental observation of the ESs provides additional support to the enhanced intermolecular interaction picture, which underlies the large mechanical stability of the chains observed experimentally.

Our results make a direct connection between concerted proton tunneling and the two signal characteristics of the symmetric chains: their enhanced mechanical stability, and the appearance of in-gap end-states. Moreover, this work demonstrates that NQE cause the emergence of electronic states at the Fermi level, a high proton tunneling rate and strong electron-proton coupling, which lead to the delocalization of π -electrons within the molecular chain. These phenomena are relevant to the ingredients used to establish the high-temperature

superconducting state recently observed in high-pressure hydrates,^{28,29} and it indicates that the strength of hydrogen bonds may be enhanced close to covalency³⁰ due to NQEs. We believe that these findings will stimulate further investigation of nuclear quantum phenomena including a search for similar systems beyond 1D where concerted proton motion and enhanced proton-coupled electron transfer strongly affect their collective mechanical and electronic properties.

References

1. Benoit, M., Marx, D. & Parrinello, M. Tunnelling and zero-point motion in high-pressure ice. *Nature* **392**, 258–261 (1998).
2. Horiuchi, S. *et al.* Above-room-temperature ferroelectricity in a single-component molecular crystal. *Nature* **463**, 789–792 (2010).
3. Frank, R. A. W., Titman, C. M., Pratap, J. V., Luisi, B. F. & Perham, R. N. A molecular switch and proton wire synchronize the active sites in thiamine enzymes. *Science* **306**, 872–876 (2004).
4. Salna, B., Benabbas, A., Sage, J. T., Van Thor, J. & Champion, P. M. Wide-dynamic-range kinetic investigations of deep proton tunnelling in proteins. *Nat. Chem.* **8**, 874–880 (2016).
5. Li, X. Z., Walker, B. & Michaelides, A. Quantum nature of the hydrogen bond. *Proc. Natl. Acad. Sci. U. S. A.* **108**, 6369–6373 (2011).
6. Guo, J. *et al.* Nuclear quantum effects of hydrogen bonds probed by tip-enhanced inelastic electron tunneling. *Science* **352**, 321–325 (2016).
7. Wang, L., Fried, S. D., Boxer, S. G. & Markland, T. E. Quantum delocalization of protons in the hydrogen-bond network of an enzyme active site. *Proc. Natl. Acad. Sci. U. S. A.* **111**, 18454–18459 (2014).
8. Bove, L. E., Klotz, S., Paciaroni, A. & Sacchetti, F. Anomalous Proton Dynamics in Ice at Low Temperatures. *Phys. Rev. Lett.* **103**, 165901 (2009).
9. Lin, L., Morrone, J. A. & Car, R. Correlated Tunneling in Hydrogen Bonds. *J. Stat. Phys.* **145**, 365–384 (2011).
10. Drechsel-Grau, C. & Marx, D. Quantum simulation of collective proton tunneling in hexagonal ice crystals. *Phys. Rev. Lett.* **112**, 148302 (2014).
11. Gross, L. *et al.* The Chemical Structure of a Molecule Resolved by Atomic Force Microscopy.

- Science* **325**, 1110–1114 (2009).
12. Jelinek, P. High resolution SPM imaging of organic molecules with functionalized tips. *J. Phys. Condens. Matter* **29**, 343002 (2017).
 13. Meng, X. *et al.* Direct visualization of concerted proton tunnelling in a water nanocluster. *Nat. Phys.* **11**, 235–239 (2015).
 14. Pascal, S. & Siri, O. Benzoquinonediimine ligands: Synthesis, coordination chemistry and properties. *Coord. Chem. Rev.* **350**, 178–195 (2017).
 15. Siri, O., Braunstein, P., Rohmer, M. M., Bénard, M. & Welter, R. Novel ‘Potentially Antiaromatic’, Acidichromic Quinonediimines with Tunable Delocalization of Their 6π -Electron Subunits. *J. Am. Chem. Soc.* **125**, 13793–13803 (2003).
 16. Dähne, S. & Leupold, D. Coupling Principles in Organic Dyes. *Angew. Chemie Int. Ed. English* **5**, 984–993 (1966).
 17. Rumpel, H. & Limbach, H. H. NMR Study of Kinetic HH/HD/DD Isotope, Solvent, and Solid-State Effects on the Double Proton Transfer in Azophenine. *J. Am. Chem. Soc.* **111**, 5429–5441 (1989).
 18. Nietzki, R. & Hagenbach, E. Ueber Tetramidobenzol und seine Derivate. *Berichte der Dtsch. Chem. Gesellschaft* **20**, 328–338 (1887).
 19. Audi, H. *et al.* Extendable nickel complex tapes that reach NIR absorptions. *Chem. Commun.* **50**, 15140–15143 (2014).
 20. Griffiths, D. J. & Schroeter, D. F. *Introduction to Quantum Mechanics*. (Cambridge University Press, 2018). doi:10.1017/9781316995433
 21. Gross, L. *et al.* Bond-order discrimination by atomic force microscopy. *Science* **337**, 1326–1329 (2012).
 22. de Oteyza, D. G. *et al.* Direct Imaging of Covalent Bond Structure in Single-Molecule Chemical Reactions. *Science* **340**, 1434–1437 (2013).
 23. Hapala, P. *et al.* Mapping the electrostatic force field of single molecules from high-resolution scanning probe images. *Nat. Commun.* **7**, 11560 (2016).
 24. de la Torre, B. *et al.* Non-covalent control of spin-state in metal-organic complex by positioning on N-doped graphene. *Nat. Commun.* **9**, 2831 (2018).
 25. Mendieta-Moreno, J. I. *et al.* Fireball / amber: An efficient local-orbital DFT QM/MM method for

- biomolecular systems. *J. Chem. Theory Comput.* **10**, 2185–2193 (2014).
26. Huynh, M. H. V. & Meyer, T. J. Proton-coupled electron transfer. *Chem. Rev.* **107**, 5004–5064 (2007).
 27. Lewis, J. P. *et al.* Advances and applications in the FIREBALL ab initio tight-binding molecular-dynamics formalism. *Phys. Status Solidi Basic Res.* **248**, 1989–2007 (2011).
 28. Drozdov, A. P., Erements, M. I., Troyan, I. A., Ksenofontov, V. & Shylin, S. I. Conventional superconductivity at 203 kelvin at high pressures in the sulfur hydride system. *Nature* **525**, 73–76 (2015).
 29. Drozdov, A. P. *et al.* Superconductivity at 250 K in lanthanum hydride under high pressures. *Nature* **569**, 528–531 (2019).
 30. Grabowski, S. J. What is the covalency of hydrogen bonding? *Chem. Rev.* **111**, 2597–2625 (2011).
 31. Blum, V. *et al.* Ab initio molecular simulations with numeric atom-centered orbitals. *Comput. Phys. Commun.* **180**, 2175–2196 (2009).
 32. Becke, A. D. A new mixing of Hartree-Fock and local density-functional theories. *J. Chem. Phys.* **98**, 1372–1377 (1993).
 33. Stephens, P. J., Devlin, F. J., Chabalowski, C. F. & Frisch, M. J. Ab Initio Calculation of Vibrational Absorption and Circular Dichroism Spectra Using Density Functional Force Fields. *J. Phys. Chem.* **98**, 11623–11627 (1994).
 34. Tkatchenko, A. & Scheffler, M. Accurate molecular van der Waals interactions from ground-state electron density and free-atom reference data. *Phys. Rev. Lett.* **102**, 073005 (2009).
 35. Heinz, H., Lin, T. J., Kishore Mishra, R. & Emami, F. S. Thermodynamically consistent force fields for the assembly of inorganic, organic, and biological nanostructures: The INTERFACE force field. *Langmuir* **29**, 1754–1765 (2013).
 36. Lee, C., Yang, W. & Parr, R. G. Development of the Colle-Salvetti correlation-energy formula into a functional of the electron density. *Phys. Rev. B* **37**, 785–789 (1988).
 37. Grimme, S., Ehrlich, S. & Goerigk, L. Effect of the damping function in dispersion corrected density functional theory. *J. Comput. Chem.* **32**, 1456–1465 (2011).
 38. Kapil, V. *et al.* i-PI 2.0: A universal force engine for advanced molecular simulations. *Comput. Phys. Commun.* **236**, 214–223 (2019).
 39. Plimpton, S. Fast Parallel Algorithms for Short-Range Molecular Dynamics. *J. Comput. Phys.*

- 117**, 1–19 (1995).
40. Kumar, S., Rosenberg, J. M., Bouzida, D., Swendsen, R. H. & Kollman, P. A. THE weighted histogram analysis method for free-energy calculations on biomolecules. I. The method. *J. Comput. Chem.* **13**, 1011–1021 (1992).
 41. Hapala, P. *et al.* Mechanism of high-resolution STM/AFM imaging with functionalized tips. *Phys. Rev. B* **90**, 085421 (2014).
 42. Peng, J. *et al.* Weakly perturbative imaging of interfacial water with submolecular resolution by atomic force microscopy. *Nat. Commun.* **9**, 122 (2018).

Figures

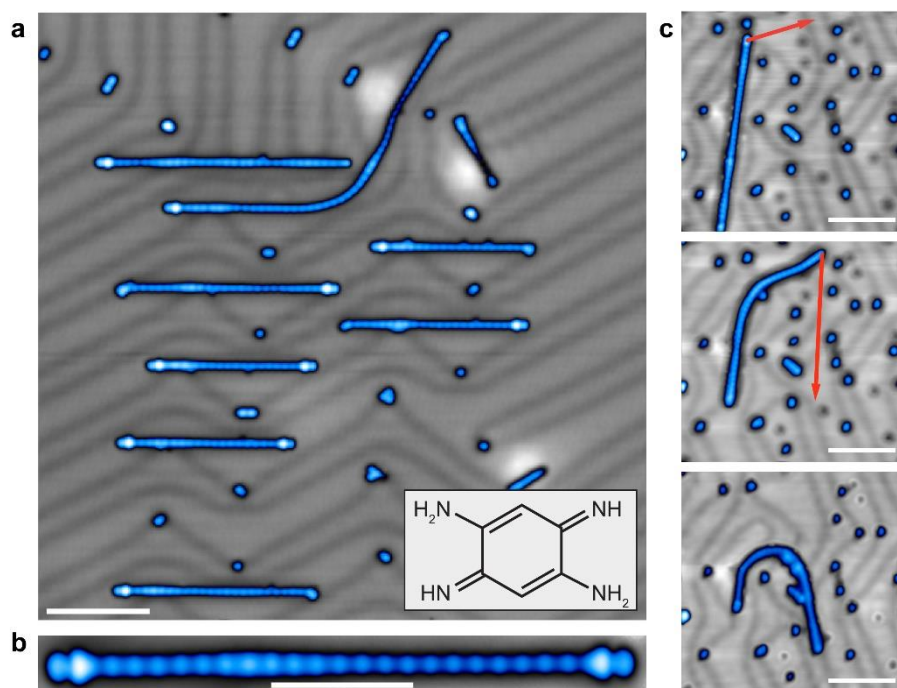


Figure 1: *a) Representative overview STM image of molecular chains and single molecule species. (50 mV, 10 pA, scale bar 10nm). Inset: 2,5-diamino-1,4-benzoquinonediimine (DABQDI) structure. b) Close-up STM image of the symmetric chain with characteristic bright spots at the ends. (30 mV, 5 pA, scale bar 5 nm) c) From top to bottom: sequentially acquired STM images of chain manipulation experiment. Red arrows represent the probe movement after contacting the chain end (procedure detailed in Methods). (all images 100 mV, 10 pA, scale bars 10 nm).*

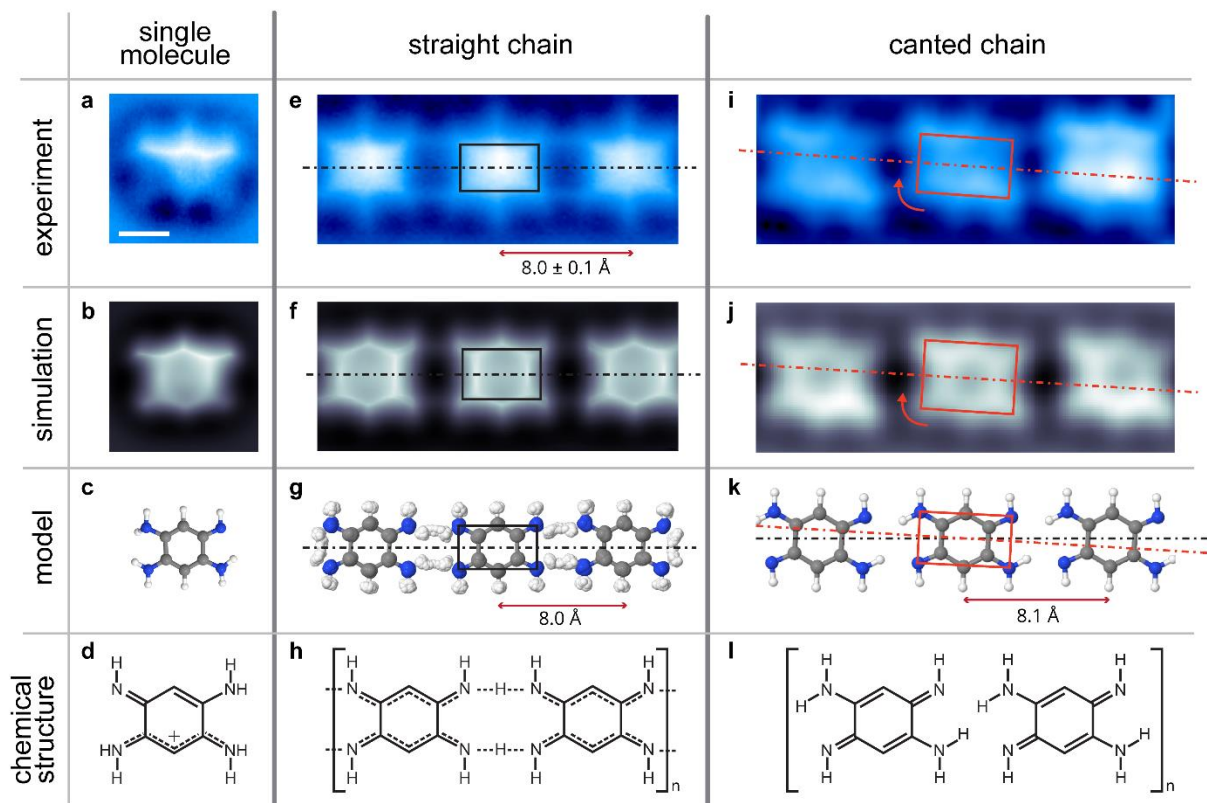


Figure 2: Comparison between experimentally acquired high resolution AFM images of the observed molecular species and their respective simulated high resolution AFM images based on the calculated models (DFT, for c) and k). a) - d) Single molecule with one additional proton, that impedes subsequent chain growth. e)- h) Hydrogen bonded symmetric chain with concerted proton tunneling. Molecular units are symmetric around the chain axis. Model (g) calculated by PIMD at the transition state. i)- l) Hydrogen bonded canted chain (no proton tunneling). Molecules are canted with respect to the main axis and distinct contrast difference between imine and amine groups is visible.

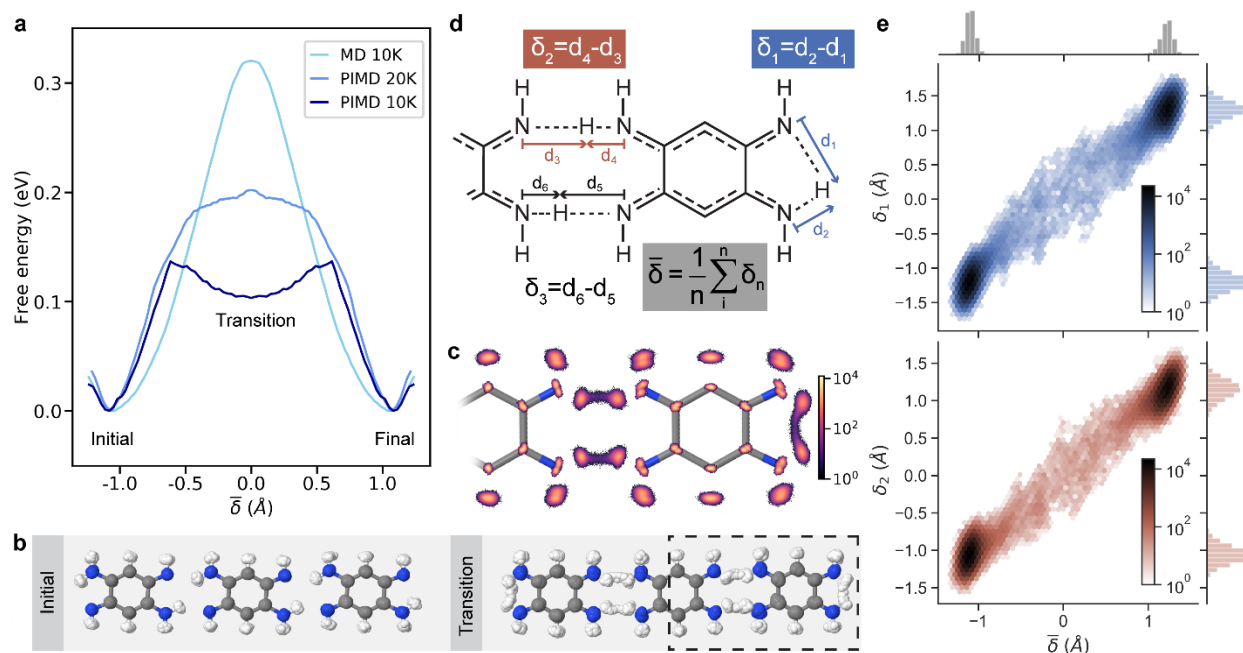


Figure 3: *a) Free energy curve of the proton transfer calculated using classical MD at 10 K (cyan), Path Integral MD at 10 K (light blue) and Path Integral MD at 20 K (dark blue) with the average $\bar{\delta}$ of all hydrogen bonds as the reaction coordinate. b) PIMD structure for $\delta = -1 \text{ \AA}$ (initial) and $\delta = 0 \text{ \AA}$ (transition) c) 2D histogram of atomic density projected in the plane of the molecules at the transition state. d) Scheme of δ reaction coordinates. e) Correlation between the average delta and δ_2 (intra) and δ_1 (edge) with 2D distribution in logarithmic scale and marginal distributions in linear scale, respectively.*

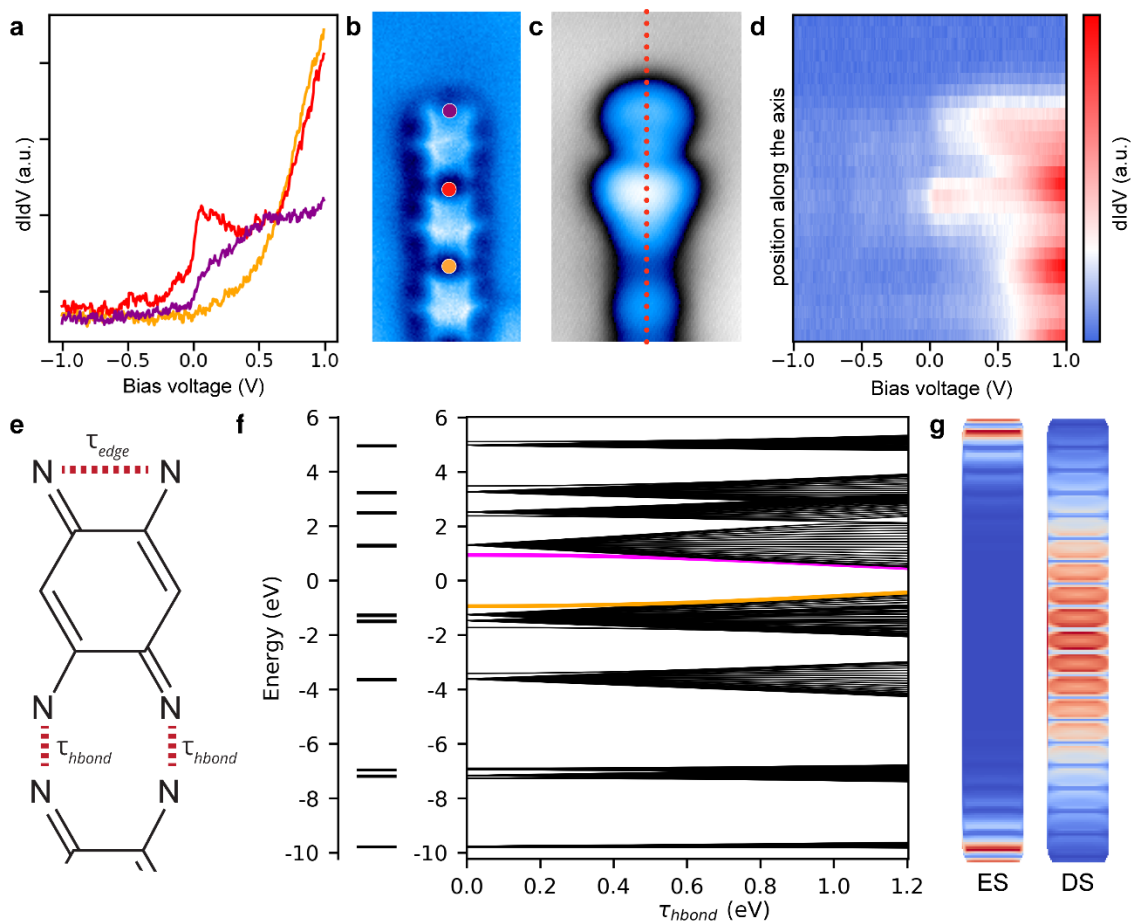
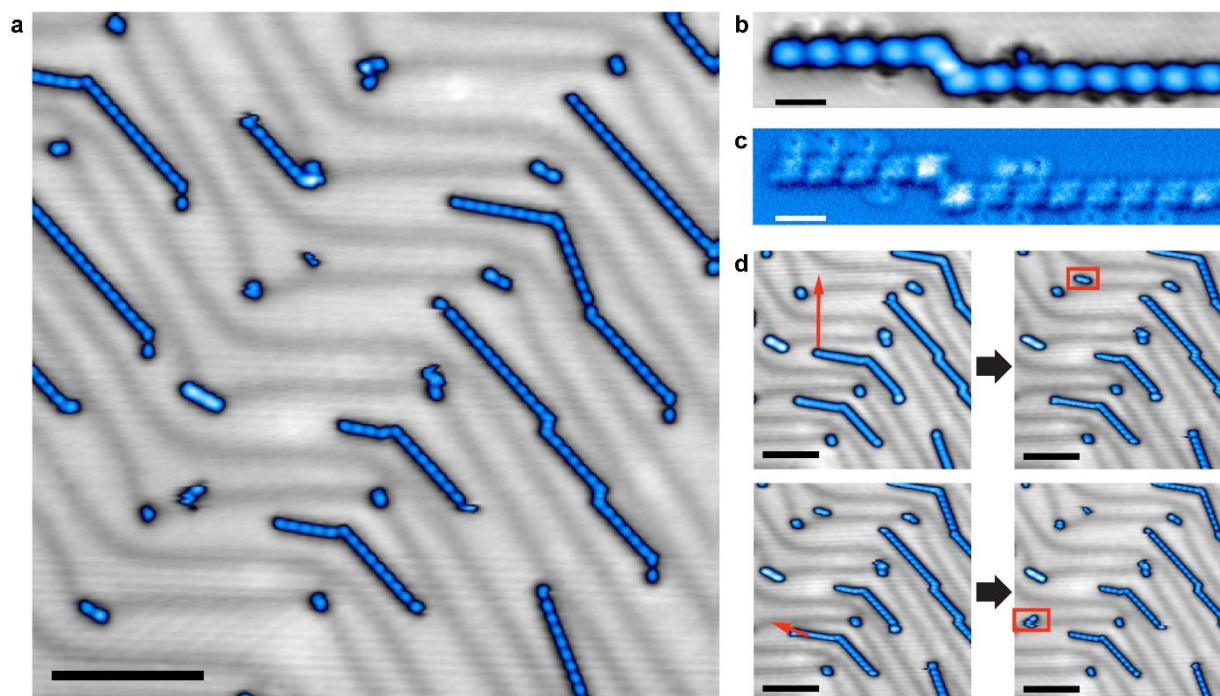
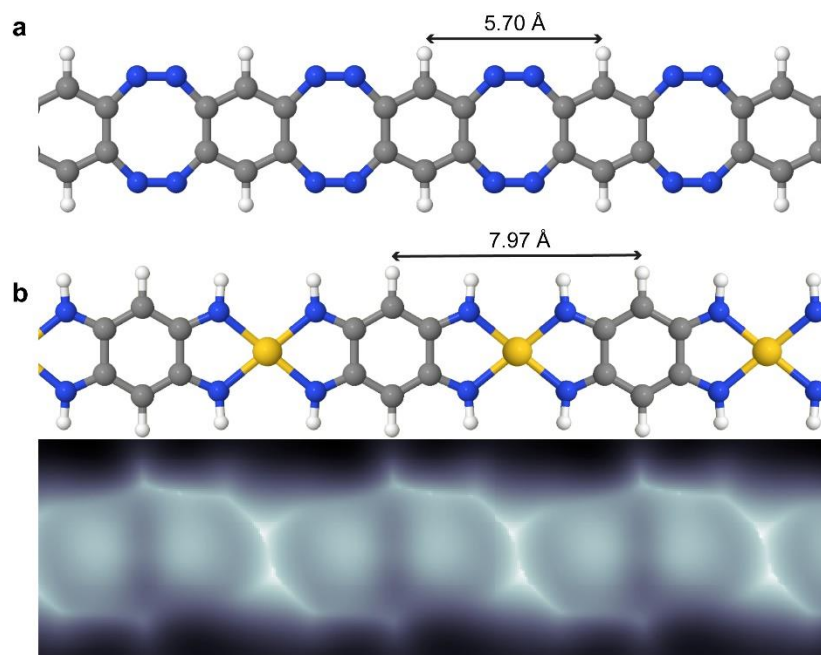


Figure 4: a) Selected point STS spectra, taken at positions marked in b), showing the presence of the in gap electronic state. b) Representative experimental high resolution AFM image of the chain end. c) Representative experimental STM image of the chain end. (30mV, 10pA) d) Map of STS spectra taken along the chain axis at positions indicated in c) showing the spatial localization of the end state around the terminating molecular unit. e) Definition of coupling parameters τ_{hbond} and τ_{edge} in the tight-binding model of a molecular chain (only non-hydrogen atoms are shown as they are the sole hosts of p_z orbitals). f) The electronic spectra of single-molecule (left) and molecular chain (right) as function of parameter τ_{hbond} ($\tau_{\text{edge}} = 0.9$ eV). In-gap states highlighted in magenta and orange. g) The spatially-resolved density of edge-states (ES) and delocalized states (DS) (blue/red corresponding to low/high density).

Extended data figures and tables



Extended Data Figure 1: *a) Representative overview STM image of canted molecular chains. (140 mV, 20 pA, scale bar 10 nm) b) Close-up STM image of canted chain showing the absence of bright spots at the chain ends (140 mV, 20 pA, scale bar 1 nm). c) High resolution AFM image of the same chain showing its inner structure with visibly canted molecular units. d) STM images (140 mV, 20 pA) taken before and after two manipulation experiments. Red arrows represent the probe movement after contacting the chain end (procedure detailed in Methods). Images on the right side (after the manipulation) show apparent splitting of the chain into segments. Scale bars 10 nm.*



Extended Data Figure 2: a) DFT calculated model of a chain composed of covalently bonded molecules with periodicity 5.7 Å. b) DFT calculated model (upper) and corresponding simulated high resolution AFM image (lower) of a metal-organic chain with single Au atoms incorporated in between the molecular units. The simulated image shows a strong repulsion signal on the Au atoms.

Methods

Chain growth

The precursor molecule 2,5-diamino-1,4-benzoquinonediimines (DABQDI) was synthesized via the procedure described in the literature¹⁹. Atomically clean Au(111) was prepared by repeated Argon ion (Ar^+) sputtering/annealing cycles. Molecules were sublimed from a home-built evaporator with tantalum pocket onto the clean Au(111) thermalized to 300 K (line-of-sight distance 30 cm). To form the straight/canted chains, molecules were evaporated at 90/120 °C for 300/30 s in an ambient pressure $4 \times 10^{-10} / 2 \times 10^{-9}$ mbar (base pressure 2×10^{-10} mbar) respectively. After molecular deposition, the sample was immediately transferred to the microscope head kept at 4 K.

STM/AFM measurements

All experiments were performed in commercial ultrahigh vacuum (UHV) low-temperature microscopes with combined STM/AFM capabilities (Specs-JT Kolibri: PtIr tip, $f_0 = 1$ MHz, $Q = 120$ k, $K = 540$ kN/m and Createc-qPlus: PtIr tip, $f_0 = 30$ kHz, $Q = 50$ k, $K = 1.8$ kN/m). To manipulate the chains, the metallic tip was approached to the chain end at $V_{\text{bias}} = 5$ mV until a characteristic, abrupt change in the current channel was observed. To achieve sub-molecular resolution, the tip apex was functionalized with a CO molecule lifted from the Au(111) substrate¹¹. All STS data were acquired in constant height mode (open feedback loop) using the lock-in technique (Nanonis internal) with a bias modulation amplitude of 5 mV and frequency 932 Hz. Prior to STS data acquisition, the tips were calibrated with reference to the Au(111) Shockley surface state.

DFT Calculations

Density functional theory (DFT) calculations were performed using the FHI-AIMS code³¹ within exchange-correlation functional B3LYP^{32,33} to describe the electronic properties of the gas-phase DABQDI molecule and of its protonated form adsorbed on the Au(111) substrate using a 6x6 unit cell. In all the calculations, we employed the tight settings for the atomic basic sets. The atomic structures were thoroughly relaxed until the Hellman-Feynman forces were smaller than 10^{-3} eVÅ⁻¹. We have used the Tkatchenko-Scheffler correction³⁴ to include van der Waals interactions in the calculations. Only the Γ -point was used for integration in the Brillouin zone.

PIMD calculations

All the simulations were performed with 3 quinone molecules in local orbital DFT with local basis set Fireball code²⁷; the surface was simulated using the interface forcefield³⁵. DFT Fireball calculations used the BLYP exchange-correlation functional^{32,36} with D3 corrections³⁷. Classical MD was performed using the QM/MM method Fireball/Amber²⁵, while PIMD was performed using the i-PI software³⁸ with QM/MM interactions calculated by Fireball and LAMMPS³⁹. We have used 512 PIMD replicas at 20 K and 1024 replicas at 10 K. To see the convergence with the number of replicas, see the supplementary material.

For the PIMD QM/MM simulation, an initial minimization of 10000 steps was performed followed by a classical QM/MM of 20 000 steps with a time step of 0.5 fs. For the PIMD we started with the results of the classical QM/MM and performed 20 000 steps with a time step of 0.25 fs.

To obtain the free energy profile we performed umbrella sampling with the bias applied to the reaction coordinate of the path integral centroid configuration at 20 K and of two contracted replicas at 10 K. The free energy profile was generated using the WHAM method⁴⁰ with 5000 steps in each window and a bias force of 200 kcal/mol on the reaction coordinate.

AFM simulations

The AFM images were calculated using the probe particle model⁴¹. The parameters of the tip were chosen to mimic a CO-tip, using a quadrupole charge moment of $-0.1 \text{ e} \cdot \text{\AA}^2$,⁴² and the lateral stiffness of the CO molecule set to 0.25 Nm^{-1} . The electrostatic interaction was described in the AFM calculations using the potential calculated by DFT. To simulate the probe dynamics we used typical values of a qPlus sensor, oscillation amplitude $A = 100 \text{ pm}$, sensor stiffness $k = 3600 \text{ N/m}$ and eigenfrequency $f_0 = 30 \text{ kHz}$. The simulated AFM image, shown in Fig. 2f, is calculated as an average of AFM images of each replica of the PIMD simulations at 10 K.

Data availability

The data that support the findings of this study are available from the corresponding authors upon reasonable request.

Acknowledgements

O.S. thanks the Centre National de la Recherche Scientifique (CNRS) and the Ministère de la Recherche et des Nouvelles Technologies. This work was supported by the Czech Science Foundation (Reg. No. 18-09914 S, 20-13692X), We acknowledge CzechNanoLab Research Infrastructure supported by MEYS CR (LM2018110). P.J. acknowledges support from Praemium Academie of the CAS. O.M. was supported by the Primus16/SCI/27/247019 grant from Charles University. Computational resources were provided by the CESNET LM2015042 and the CERIT Scientific Cloud LM2015085, provided under the programme “Projects of Large Research, Development, and Innovations Infrastructures”.

Author information

Author notes

These authors contributed equally: Aleš Cahlík, Jack Hellerstedt, Jesus I. Mendieta-Moreno.

Affiliations

Institute of Physics of the Czech Academy of Sciences, Prague, Czech Republic

Aleš Cahlík, Jack Hellerstedt, Jesús I. Mendieta-Moreno, Martin Švec, V M Santhini, Karel Výborný, Pingo Mutombo, Pavel Jelínek

Faculty of Nuclear Sciences and Physical Engineering, Czech Technical University in Prague, Prague, Czech Republic

Aleš Cahlík

Regional Centre of Advanced Technologies and Materials, Palacký University, Olomouc, Czech Republic

Aleš Cahlík, Martin Švec, Pavel Jelínek

Aix Marseille Univ, CNRS, CINaM, UMR 7325, Campus de Luminy, Marseille, France

Simon Pascal, Olivier Siri

Universidad Autónoma de Madrid, Campus Cantoblanco, Madrid, Spain

Diego Soler

School of Science and Engineering, Reykjavik University, Reykjavik, Iceland

Sigurdur I. Erlingsson

Charles University, Faculty of Mathematics and Physics, Prague, Czech Republic

Ondrej Marsalek

Contributions

P.J. and O.S. conceived the project and designed the experiments. A. C., J. H., V.M. S. and M. Š. performed and analyzed the SPM experiments. S. P. and O. S. synthesized organic molecules. J.I.M., D.S., S.I.E., K.V. and P.J. performed tight bonding modelling, P.M. performed DFT and AFM calculations, J.I.M., O.M. performed PIMD calculations. J.I.M., D.S., S.I.E., K.V, O.M. and P.J interpreted theoretical results and underlying mechanism. All authors discussed the results, co-wrote and commented on the manuscript.

Corresponding authors

Correspondence to Olivier Siri or Pavel Jelínek

Ethics declarations

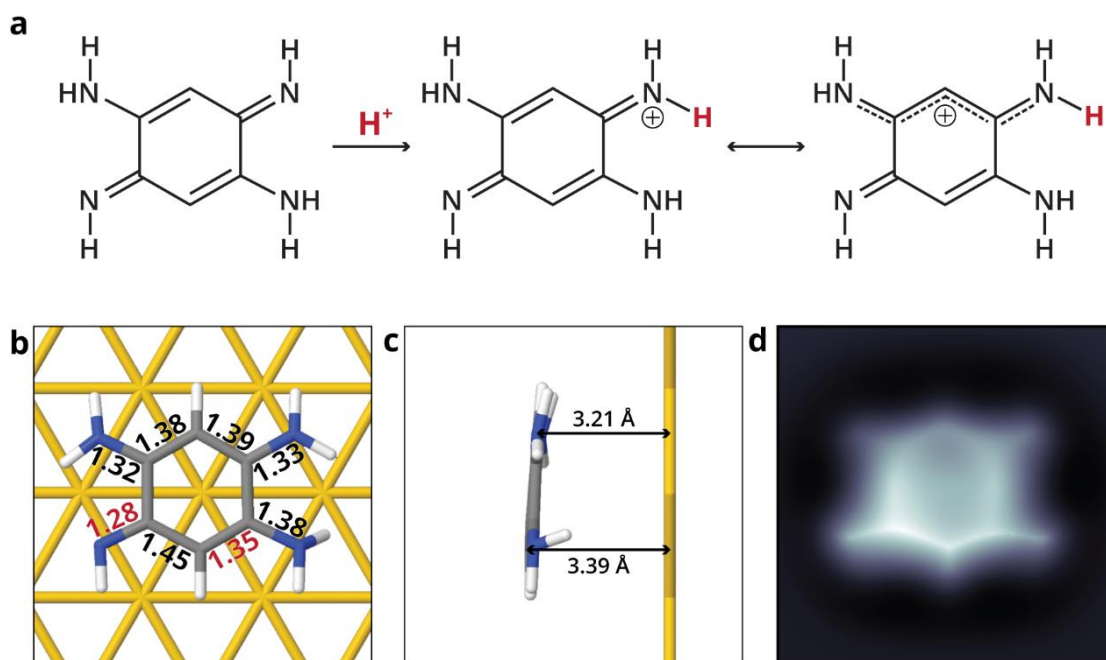
Competing interests

The authors declare no competing interests.

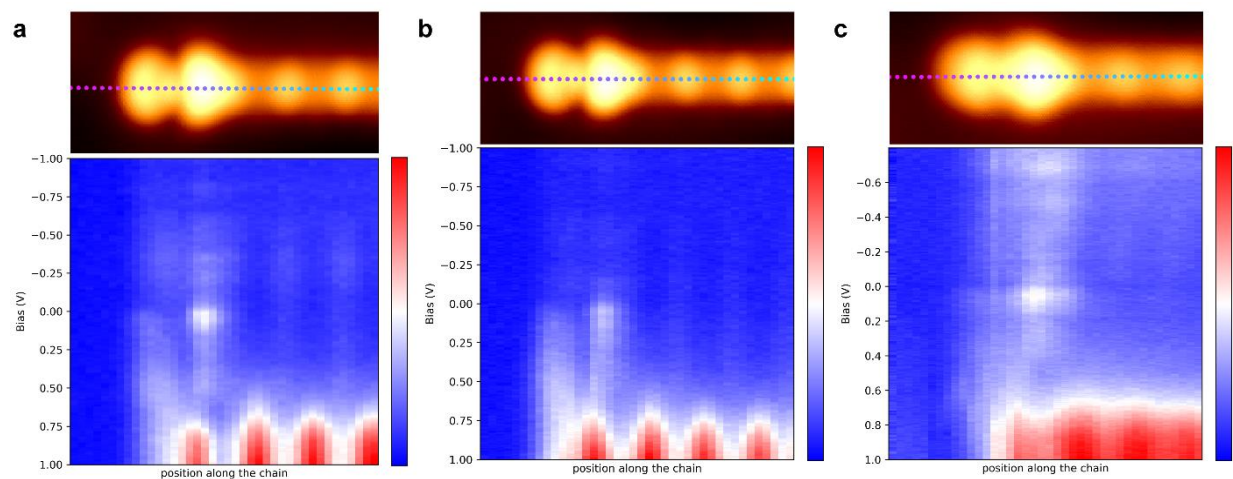
Supplementary Information

Analysis of single molecules on gold surface

As shown by Siri et al.¹⁵ hydrogenation of benzoquinonediimine ligands (see Supp. Fig. 1a) results in delocalization of one of the formerly localized 6π -electron conjugated systems (Supp. Fig. 1b). AFM image simulation (Supp. Fig. 4d) of such a hydrogenated structure agrees very well with the experimental images of single molecular species observed on the sample surface (Fig. 2a). The asymmetry in the nc-AFM signal contrast arises due to the adsorption height difference (Supp. Fig. 1c). We consider two possible sources of the additional hydrogen – either a hydrogen transferred from other molecules or residual hydrogen gas in the UHV system. In the STM overview images, we have observed step edges decorated with clusters of undistinguishable molecular residues. These could potentially be dehydrogenated molecular units, however, we were not able to fully experimentally confirm either of these scenarios.



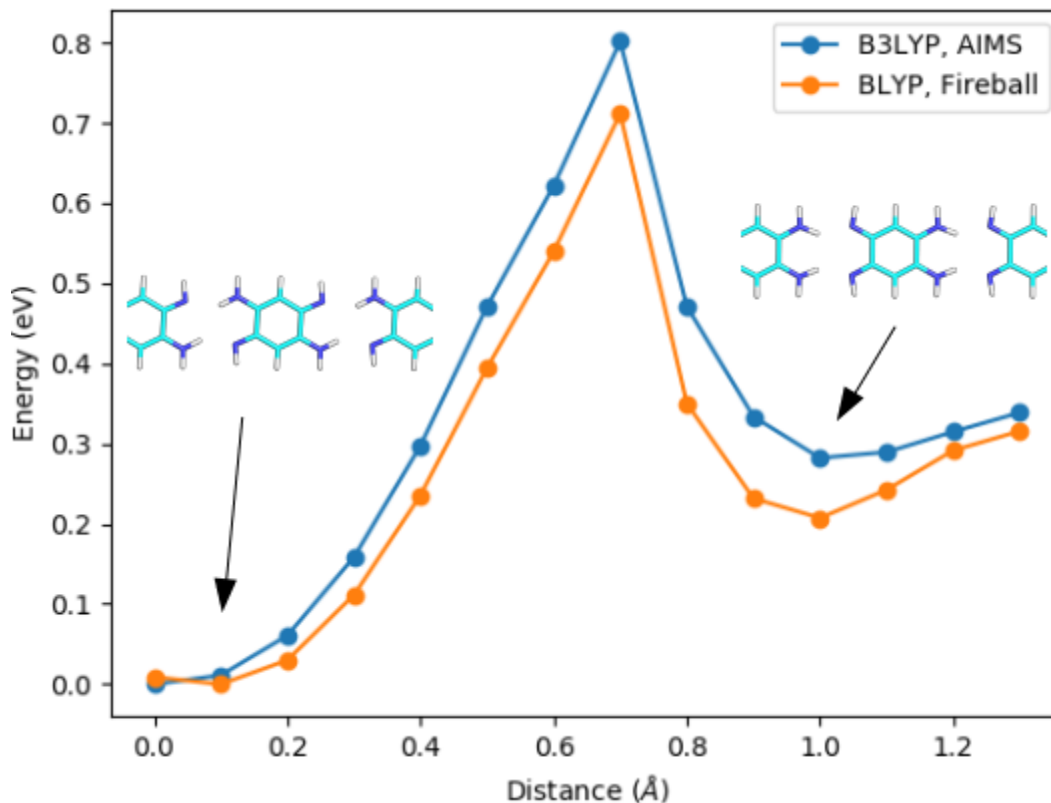
Supplementary figure 1: a) Protonation reaction of 2,5-diamino-1,4-benzoquinonediimine. b) DFT calculated structure of the protonated DABQDI. Comparison of interatomic distances confirm the delocalization of the protonated conjugated system. c) Adsorption height difference causing the AFM image contrast asymmetry. d) Simulated nc-AFM image of the protonated DABQDI molecule.



Supplementary figure 2: *a), b), c) Maps of STS spectra (bottom) taken with different metallic tips along the chain axis at positions indicated in STM image (top) showing the spatial localization of the end state around the terminating molecular unit.*

Comparison of FHI-AIMS and Fireball DFT methods

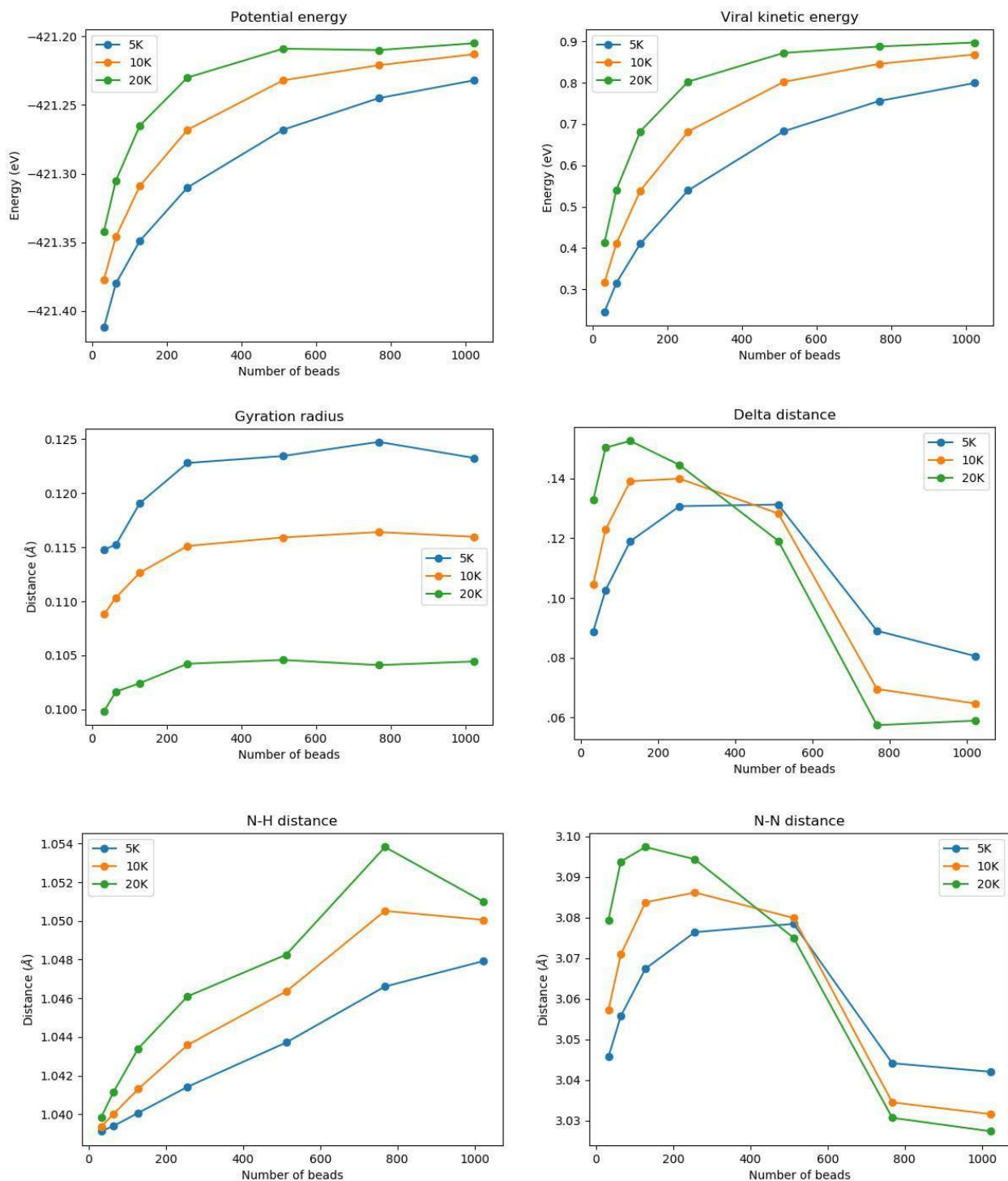
Path Integral Molecular Dynamics (PIMD) has been performed with the local orbital Fireball DFT package. To validate the accuracy of Fireball BLYP-D3 we compared it with the potential energy landscape of a single proton transfer in a periodic system calculated with the FHI-AIMS package using B3LYP-TS. Supplementary figure 3 compares the calculated energy barriers, which are similar. This justifies our use of the Fireball package to increase the conformational sample in our PIMD simulations.



Supplementary figure 3: Comparison of potential energy profiles of the single proton transfer in a periodic system obtained with FHI-AIMS B3LYP-TS (blue), and Fireball BLYP-D3 (orange) calculations.

Convergence based on the number of replicas in PIMD calculations at different temperatures

The dependence of the number of replicas with temperature has been studied for 5, 10 and 20 K, with 32, 64, 128, 256, 512, 768 and 1024 replicas for the PIMD. To ensure that the system is stable we performed 10000 steps of PIMD with a time step of 0.25 fs for each pair of values. In order to see the convergence with the number of replicas for this system we represent the average over the last 2000 steps for each case, shown in Supplementary figure 4. Based on these simulations we conclude that we can do simulations at 20 K and 10 K with 1024 replicas. The simulations at 5 K seem to need more than 1024 replicas for full convergence and the computational cost to perform free energy calculations becomes prohibitive.

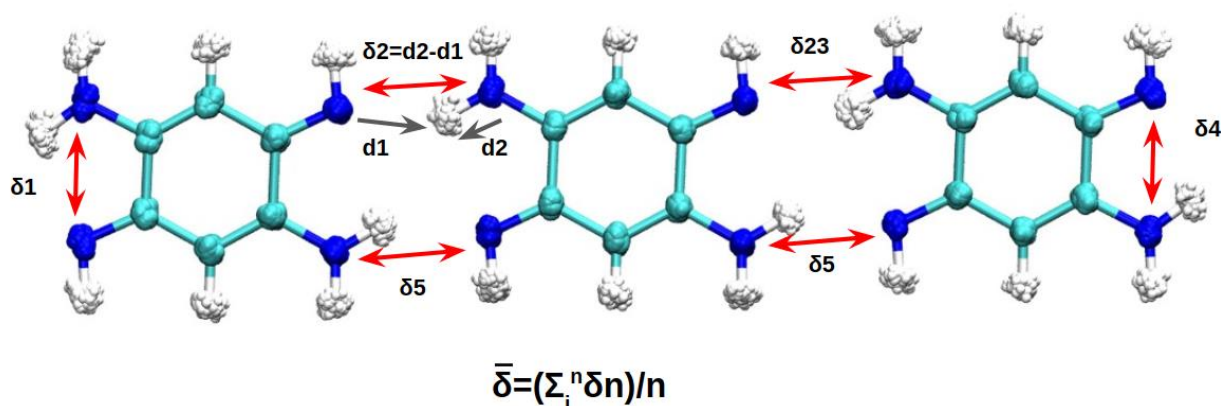


Supplementary figure 4: Evolution of the mean value for the last 2000 steps of the PIMD for potential energy, viral kinetic energy, gyration radius delta distance, N-H distance and N-N distance at different temperatures (blue 5 K, green 10 K and red 20 K) when we change the number of replicas.

Free energy calculations

Free energy profile calculations were carried out for a system consisting of three quinone molecules on the gold surface using the QM/MM scheme described below. We employed the WHAM method using 51 windows along the reaction coordinate. We have performed 3000 steps in each window with a time step of 0.25 fs.

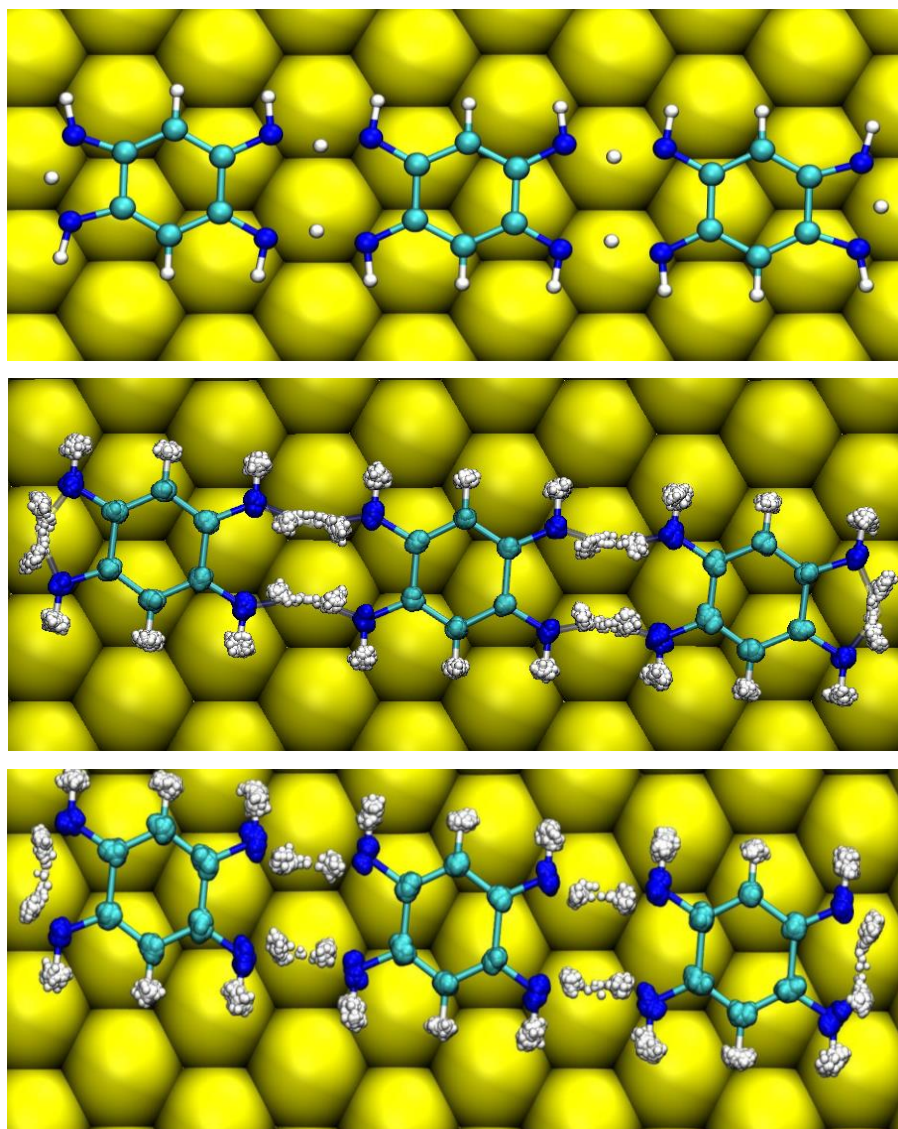
To understand the behavior of the system, we considered distinct reaction coordinates transferring the hydrogen atoms from one nitrogen to the opposite nitrogen along the H-bond. Namely, we have tested as reaction coordinates the position of just one hydrogen atom, the collective reaction coordinate (average of the positions of all hydrogens), and also a different umbrella-like restraint for each hydrogen atom (see Supplementary figure 5).



Supplementary figure 5: Scheme of the reaction coordinates used for the classical and PIMD QM/MM simulations.

The behavior of the system for the average of the δ and for six restraints is the same for PIMD simulations, consistent with the idea that coordinated proton tunneling takes place in the system. For the free energy profile at 20 K, a restraint has been added to the centroid of the ring polymer with 512 replicas. In the case of the 10 K free energy profile, a restraint has been added to two contracted replicas. This is due to the large delocalization of the ring polymer around $\delta=0$ Å, which creates hysteresis along the reaction when we apply the restraint only over the centroid. For the classical QM/MM simulations, we have to carry out the simulation restraining every

hydrogen simultaneously to obtain the same geometries that we observe in PIMD simulations. If we apply the restraint in the average δ in the classical MD simulations, we don't have a coordinated movement, but rather multiple barriers in a stepwise process. In Figure 3a of the main text the barrier for the classical MD at 10 K has been performed with a restraint on all the δ to be able to compare the energy.

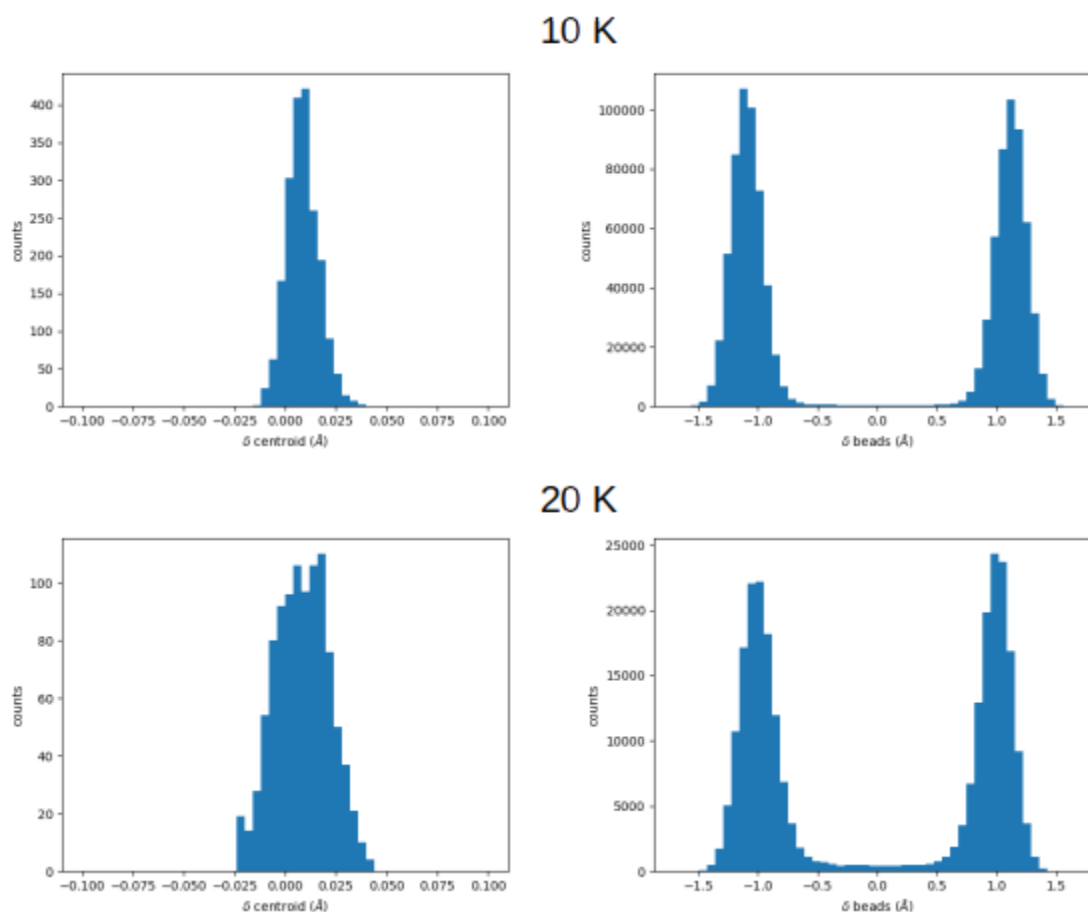


Supplementary figure 5: *Representation of the proton distribution at $\delta=0$ Å with classical MD at 10 K (top), PIMD at 20 K (middle) and PIMD at 10 K (bottom).*

In Supplementary figure 5, appreciable differences between the MD and PIMD approaches can be observed. In the classical MD simulation, the protons are located just in the middle of the hydrogen bond, while in the PIMD simulations we observe a delocalization of the hydrogens along the hydrogen bond. This difference in behaviour is responsible for the flatness of the barrier and characteristic of the deep tunneling regime. Moreover, we observe a further difference between the PIMD simulations at 10 K and 20 K.

Analysis of the concerted motion of protons

To study the correlation of the different protons we perform a 5000 step of free dynamics calculation at 10 K starting in the window corresponding to $\delta=0$ Å in the free energy profile. During the last 2000 steps of this PIMD we measured the δ coordinate of all the hydrogen bonds for the centroid trajectory and for all the 1024 replicas of our system. During this simulation the average δ stays around 0 Å but we can see that the distribution of the delta value for the replicas' trajectories has two clear peaks for each protonation state, as shown in Supplementary figure 7.

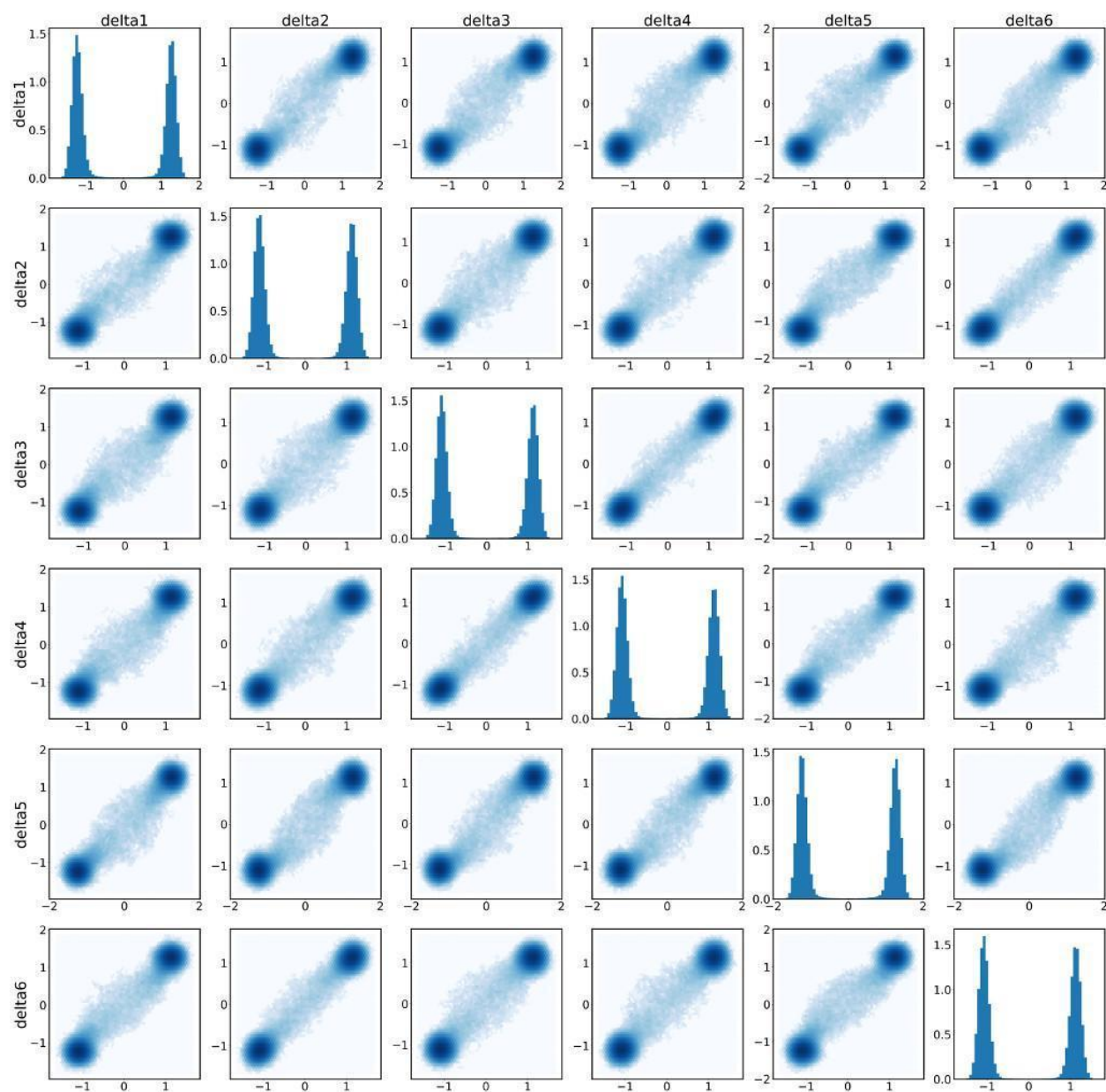


Supplementary figure 7: Histogram of the distribution of the δ_2 value for the centroid (left images), the δ_2 for all the replicas (right images) at 10 K (top images) and 20 K (bottom images).

When the centroid coordinate in the PIMD simulation has a value of $\delta=0$ Å the state of the

system is actually a combination of the two possible protonation states. In this way the system is able to maintain the π -conjugation in each of the protonated states.

Supplemental figure 8 displays histogram of distribution of δ -coordinates of all hydrogen atoms involved in the proton transfer mechanism obtained from the PIMD simulations at 10 K. The distribution shows strong correlation between positions of all hydrogen atoms, which is dictated by conservation of the π -conjugation. This demonstrates that the proton transfer is concerted.



Supplementary figure 8: Plot with the correlation between the δ -coordinates and the histogram with the distribution of each δ in the diagonal. δ_1 and δ_4 correspond to hydrogens in the edges and $\delta_2, \delta_3, \delta_5, \delta_6$ are hydrogens in the middle of the chain.

Another way to see the correlation is to calculate the Pearson correlation coefficients that measure how far the reaction coordinates δ_i are from a linear correlation where 1.0 corresponds to perfect linear correlation and 0.0 means complete lack of correlation. In this matrix, representation we can see these values between each set of δ -coordinates in the PIMD simulations of the molecular trimer. The positions in the matrix correspond to the sub-index of the reaction coordinates δ shown in Supplementary figure 5.

	δ_1	δ_2	δ_3	δ_4	δ_5	δ_6
δ_1	1.000	0.9826	0.9821	0.9823	0.9831	0.9833
δ_2	0.9826	1.000	0.9854	0.9840	0.9825	0.9866
δ_3	0.9821	0.9854	1.000	0.9865	0.9827	0.9854
δ_4	0.9823	0.9840	0.9865	1.000	0.9833	0.9847
δ_5	0.9831	0.9825	0.9827	0.9833	1.000	0.9832
δ_6	0.9833	0.9866	0.9854	0.9847	0.9832	1.000

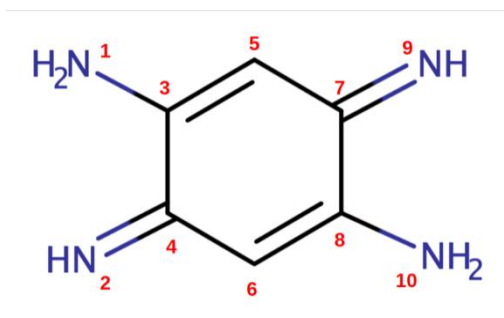
Supplementary table 1: Pearson correlation coefficients between distinct reaction coordinates δ_i obtained from the PIMD simulation.

Tight-Binding model on the molecular chain

To construct the Tight-Binding model used in our analysis, we first considered an isolated molecule in the XY-plane and constructed its Hamiltonian with Fireball in the orthonormal Löwdin basis, using the BLYP functional for the calculation. We then selected the 10x10 matrix corresponding to the π -conjugated system (the Hamiltonian elements between the pairs of Löwdin π -orbitals associated to p_z orbitals of carbon and nitrogen atoms). All the matrix elements between atoms not bonded covalently are 20 to 30 times smaller than those representing bonded atoms, so they are set to zero in our model. With p_z orbitals labelled by the number of the atom (see Fig. S9), the resulting Hamiltonian $H_{tb,0}$ is (in the units of eV):

$$\begin{pmatrix} 6.02 & 0 & 3.21 & 0 & 0 & 0 & 0 & 0 & 0 & 0 \\ 0 & 3.48 & 0 & 3.65 & 0 & 0 & 0 & 0 & 0 & 0 \\ 3.21 & 0 & 2.77 & 2.75 & 3.47 & 0 & 0 & 0 & 0 & 0 \\ 0 & 3.65 & 2.75 & 2.28 & 0 & 3.06 & 0 & 0 & 0 & 0 \\ 0 & 0 & 3.47 & 0 & 2.32 & 0 & 3.06 & 0 & 0 & 0 \\ 0 & 0 & 0 & 3.06 & 0 & 2.33 & 0 & 3.47 & 0 & 0 \\ 0 & 0 & 0 & 0 & 3.06 & 0 & 2.28 & 2.75 & 3.65 & 0 \\ 0 & 0 & 0 & 0 & 0 & 3.47 & 2.75 & 2.77 & 0 & 3.21 \\ 0 & 0 & 0 & 0 & 0 & 0 & 3.65 & 0 & 3.46 & 0 \\ 0 & 0 & 0 & 0 & 0 & 0 & 0 & 3.21 & 0 & 6.02 \end{pmatrix}$$

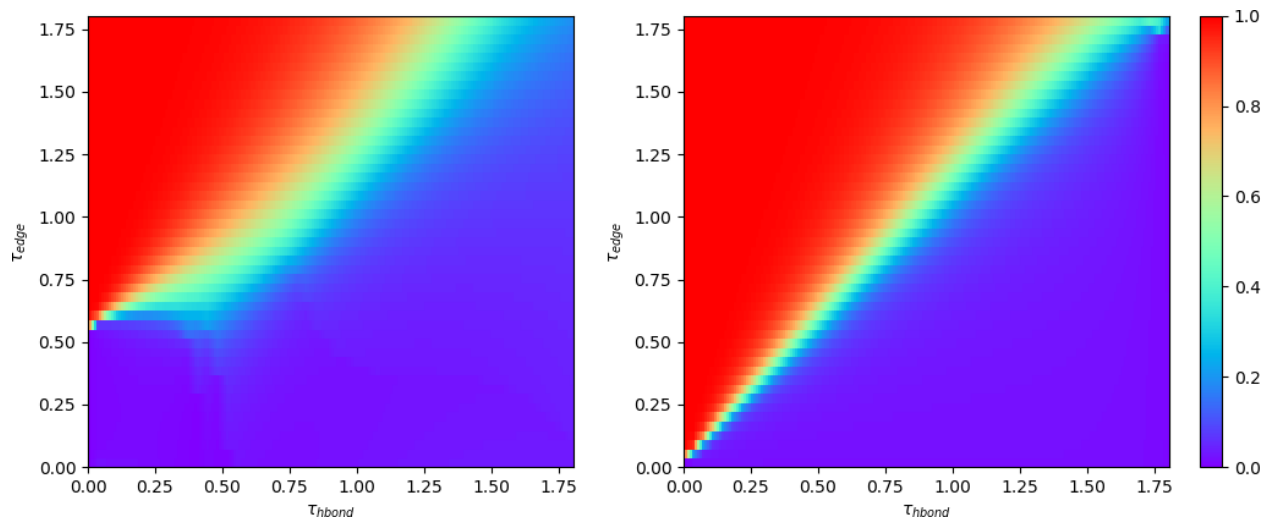
Supplementary table 2: *Tight-binding Hamiltonian of the molecular unit obtained from Fireball DFT calculations. Labeling of sites with the molecular unit is represented in Supplementary figure 9.*



Supplementary figure 9: Labeling used for the tight-binding Hamiltonian.

To study a chain consisting of multiple units, we constructed a block matrix built up from replicas of $H_{tb,0}$ and add the hoppings associated to the hydrogen bonds connecting the neighboring units, τ_{hbond} (i.e. sites 9 and 1 of two adjacent blocks are coupled and similarly, sites 2 and 10). We assume that proton tunneling enhances this coupling compared to the '*frozen-proton hydrogen bond*' case and also allows for a direct link between the terminal nitrogen pairs of the chain: a hopping τ_{edge} between the pairs of nitrogen atoms 1&2 in the first and 9&10 in the last molecule is added. We then proceed to explore our model over a wide range of values of τ_{edge} and τ_{hbond} . The reason for this is that, at very low temperatures, the hydrogen transfer rate is heavily affected by nuclear quantum corrections, and thus cannot be correctly estimated by means of a DFT calculation relying on Born-Oppenheimer approximation. We find that for situations in which $\tau_{edge} > \tau_{hbond}$, edge states appear in gap as HOMO, HOMO-1, LUMO and LUMO+1 molecular levels, for values of τ_{edge} and τ_{hbond} which are small compared to the rest of the non-zero matrix elements ($\sim 0.5-1.5$ eV), but still larger than usual hopping for atoms bonded by hydrogen bonds (0.1 eV). This corroborates the importance of quantum nuclear effects at low temperature. The tunneling regime of the hydrogens leads to an effective interaction between the nitrogen atoms which is comparable in strength to a covalent bond.

Supplementary figure 10 summarizes the weights over the edges (defined as the two first and the last two molecules in the chain) of the HOMO and LUMO orbitals. The horizontal axis is the value of the hopping τ_{hbond} , the vertical one is τ_{edge} , and the color represents the projection of the wave function of the eigenstates on the sites that we identify as the edge regions. We also remark that our tight-binding model with $\tau_{edge}=0$ implies the existence of edge states related to the topologically-nontrivial states in the Su-Schrieffer-Heeger model,⁴³ but these never occur close to the Fermi level.



Supplementary figure 10: Projection of the HOMO (a) and LUMO (b) to the edge region in our tight-binding model. Red color corresponds to the parameter region (τ_{edge} , τ_{hbond}) where the edge states occur.

Supplementary References

43. Su, W. P., Schrieffer, J. R. & Heeger, A. J. Soliton excitations in polyacetylene. *Phys. Rev. B* **22**, 2099–2111 (1980).